Mineralogical Magazine (2023), **87**, 711–718
doi:10.1180/mgm.2023.43

CAMBRIDGE UNIVERSITY PRESS

Article

Napoliite, Pb_2OFCl, a new mineral from Vesuvius volcano, and its relationship with dimorphous rumseyite

Anatoly V. Kasatkin[1], Oleg I. Siidra[2,3], Fabrizio Nestola[4], Igor V. Pekov[5], Atali A. Agakhanov[1], Natalia N. Koshlyakova[5], Nikita V. Chukanov[6], Evgeny V. Nazarchuk[2], Simone Molinari[7] and Manuela Rossi[8]

[1]Fersman Mineralogical Museum of the Russian Academy of Sciences, Leninsky Prospekt 18-2, 119071 Moscow, Russia; [2]Department of Crystallography, Institute of Earth Sciences, St. Petersburg State University, University emb. 7/9, 199034 St. Petersburg, Russia; [3]Kola Science Center, Russian Academy of Sciences, Apatity, Murmansk Region, 184200, Russia; [4]Dipartimento di Geoscienze, Università di Padova, Via Gradenigo 6, I-35131, Padova, Italy; [5]Faculty of Geology, Moscow State University, Vorobievy Gory, 119991 Moscow, Russia; [6]Federal Research Center of Problems of Chemical Physics and Medicinal Chemistry of the Russian Academy of Sciences, 142432 Chernogolovka, Moscow region, Russia; [7]Museo della Natura e dell'Uomo, Sezione di Mineralogia Alessandro Guastoni, Università degli Studi di Padova, Via Giotto 1, I-35121, Padova, Italy; and [8]Dipartimento di Scienze della Terra dell'Ambiente e delle Risorse, Università degli Studi di Napoli Federico II, via Cintia 4, I-80126, Napoli, Italy

Abstract

Napoliite, ideally Pb_2OFCl, is a new fluoroxychloride mineral found in a specimen from a fumarole formed subsequent to the 1944 eruption of Vesuvius volcano, Naples Province, Italy. It occurs as well-shaped lamellar crystals up to $0.25 \times 0.25 \times 0.01$ mm typically forming clusters up to 0.4×0.4 mm on the surface of volcanic scoria in association with anglesite, artroeite, atacamite, calcioaravaipaite, cerussite, challacolloite, cotunnite, hephaistosite, manuelarossiite, matlockite and susannite. Napoliite is colourless with white streak and adamantine lustre. It is brittle and has a laminated fracture. Cleavage is perfect on {001}. $D_{calc} = 7.797$ g cm^{-3}. The calculated mean refractive index is 2.10. Chemical composition (wt.%, electron microprobe) is: PbO 91.71, F 3.89, Cl 7.34, −O=(F+Cl) −3.30, total 99.64. The empirical formula calculated on the basis of 3 anions is $Pb_{1.999}O_{0.997}F_{0.996}Cl_{1.007}$. Raman spectroscopy confirms the absence of OH^- groups and H_2O molecules in the mineral. Napoliite is tetragonal, space group $P4_2/mcm$, $a = 5.7418(11)$, $c = 12.524(4)$ Å, $V = 412.9(2)$ Å^3 and $Z = 4$. The strongest lines of the powder X-ray diffraction pattern [d, Å (I, %) (hkl)] are: 3.860 (85) (111); 3.139 (20) (004); 2.914 (100) (113); 2.866 (63) (200); 2.118 (19) (204); 2.027 (19) (220); 1.665 (20) (313); and 1.642 (23) (117). The crystal structure was refined to $R_1 = 0.024$ for 222 reflections with $F > 4\sigma(F)$. It is based on lead oxide blocks derived from that of litharge PbO, which alternate with layers of chloride ions. Napoliite represents a new structure type with a unique order/disorder pattern of fluorine and oxygen atoms. The new mineral is dimorphous with rumseyite. It is named after the city of Naples (Napoli in Italian).

Keywords: napoliite; new mineral; lead oxyhalides; crystal structure; rumseyite; fumarole sublimate; Vesuvius volcano

(Received 2 May 2023; accepted 28 May 2023; Accepted Manuscript published online: 14 June 2023; Associate Editor: Elena Zhitova)

Introduction

The Vesuvius volcano, located ~9 km east of Naples in Campania, Italy is one of the world's most famous geological objects and attracts millions of visitors each year. It is also one of the most studied volcanoes and a world-class mineralogical location. To date, the Somma–Vesuvius volcanic complex is the type locality of 68 mineral species. While most of them have 'grandfathered' status, several minerals have been described more recently as a result of new finds or the re-examination of old samples facilitated by progress in X-ray diffraction and other analytical techniques. Among them are d'ansite-(Mn), $Na_{21}Mn^{2+}(SO_4)_{10}Cl_3$ (Demartin *et al.*, 2012), ghiaraite, $CaCl_2{\cdot}4H_2O$ (Rossi *et al.*, 2014), parascandolaite, $KMgF_3$ (Demartin *et al.*, 2014), tondiite, $Cu_3Mg(OH)_6Cl_2$ (Malcherek *et al.*, 2014), verneite, $Na_2Ca_3Al_2F_{14}$ (Balić-Žunić *et al.*, 2018), sbacchiite, Ca_2AlF_7 (Campostrini *et al.*, 2019), and paradimorphite, As_4S_3 (Campostrini *et al.*, 2022). Herein, we report another new mineral, napoliite named after the city of Naples (Napoli in Italian).

The new mineral, its name and symbol (Npi) have been approved by the Commission on New Minerals, Nomenclature and Classification of the International Mineralogical Association (IMA2022–073; Kasatkin *et al.*, 2023). The holotype specimen is deposited in the collections of the Fersman Mineralogical Museum of the Russian Academy of Sciences, Moscow, Russia with the registration number 5885/1. A part of the holotype specimen is deposited in the collections of the Sezione di Mineralogia "Alessandro Guastoni" of the Museo della Natura e dell'Uomo, University of Padova, under catalogue number MMP M23222.

Occurrence and mineral association

The Somma–Vesuvius complex (Campania region, Italy) is characterised by complex magmatism and volcanism (Lima *et al.*, 2007; Alfano and Parascaldola, 2015; Sbrana *et al.*, 2020; Melluso *et al.*, 2022); it is a polygenic stratovolcano with strong

Corresponding author: Anatoly V. Kasatkin; Email: anatoly.kasatkin@gmail.com
Cite this article: Kasatkin A.V., Siidra O.I., Nestola F., Pekov I.V., Agakhanov A.A., Koshlyakova N.N., Chukanov N.V., Nazarchuk E.V., Molinari S. and Rossi M. (2023) Napoliite, Pb_2OFCl, a new mineral from Vesuvius volcano, and its relationship with dimorphous rumseyite. *Mineralogical Magazine* **87**, 711–718. https://doi.org/10.1180/mgm.2023.43

eruption variability in terms of style, cyclicity and magma composition. During the last 3.5 ka effusive lava flows and scoria eruptions were alternated to highly explosive Plinian eruptions of pumice and ash, with pyroclastic flows and surges. All exposed lavas refer to the recent activity between A.D. 1631 and 1944 (Santacroce *et al.*, 2008; Sbrana *et al.*, 2020). Since 1944, Vesuvius has been quiescent, with only moderate seismicity and fumarolic activity.

The last eruption dating back to 1944, began on March 18th and ended on the 29th of the same month, marked the transition from an open conduit to a closed conduit state. The eruption took place during wartime that precluded the collecting of specimens after the eruption and their investigation. Antonio Parascandola was the only person who studied the mineralogy of these fumaroles between 1948 and 1960, when temperatures decreased from a maximum of 800°C in 1950 to ~460°C in 1960s (Parascandola, 1951, 1960, 1961). His studies revealed the presence of about ten mineral species new for Vesuvius.

In recent times, the systematic study of fumarolic minerals formed after the 1944 eruption has been undertaken by a joint team of scientists from the Department of Chemistry of the University of Milan and the Naples section of the National Institute of Geophysics and Volcanology – Vesuvius Observatory (see, e.g. Campostrini and Gramaccioli, 2005; Russo and Campostrini, 2011; Russo *et al.*, 2014) that resulted in a discovery of several rare minerals previously unknown at this locality, such as ammineite, artroeite, caledonite, fluornatrocoulsellite, gearksutite, hemimorphite and matlockite, and the description of two new species – parascandolaite, $KMgF_3$ (Demartin *et al.*, 2014) and sbacchiite, Ca_2AlF_7 (Campostrini *et al.*, 2019).

Napoliite, therefore, is the third new mineral discovered in the material from fumaroles of the 1944 eruption. The sample of lava scoria where napoliite occurs was collected by one of the authors (MR) in early 2010s from a large fragment located at the eastern rim of the 'Gran Cono' crater. Napoliite overgrows volcanic scoria and is associated with anglesite, artroeite, atacamite, calcioaravaipaite, cerussite, challacolloite, cotunnite, hephaistosite, matlockite, susannite and the recently discovered new mineral manuelarossiite $PbCaAlF_7$ (IMA2022–097, Nestola *et al.*, 2023). Hephaistosite and susannite are of special interest, as both of them were found on Vesuvius for the first time. Hephaistosite occurs as small grains up to 0.02 mm forming a limited solid-solution series with Tl-bearing challacolloite. The most Tl-rich hephaistosite variety contains (wt.%): K 2.04, Tl 16.06, Pb 57.47, Cl 24.08, total 99.65. Its empirical formula is $(Tl_{0.58}K_{0.38})_{\Sigma 0.96}Pb_{2.04}Cl_{5.00}$. Susannite occurs as prismatic colourless crystals up to 1 mm long with adamantine lustre. Its identification is based on semi-quantitative chemical analysis (only Pb, S, C and O detected using energy-dispersive spectroscopy with a Pb to S ratio equal to 4:1) and single-crystal X-ray diffraction data. The parameters of its trigonal unit cell are: $a = 9.080(10)$, $c = 11.565(12)$ Å and $V = 826.7(15)$ Å^3.

General appearance and physical properties

Napoliite occurs as well-shaped lamellar crystals up to $0.25 \times 0.25 \times 0.01$ mm typically forming clusters up to 0.4×0.4 mm on the surface of volcanic scoria (Fig. 1). The new mineral is colourless and transparent with white streak and adamantine lustre. It is brittle and has a laminated fracture. No fluorescence is observed under long- or short-wave ultraviolet light. The hardness is ~3 on the Mohs' scale. Cleavage is perfect on {001}. The density of napoliite could not be determined due to the scarcity of available material. Density calculated using the empirical formula is 7.797 g cm^{-3}.

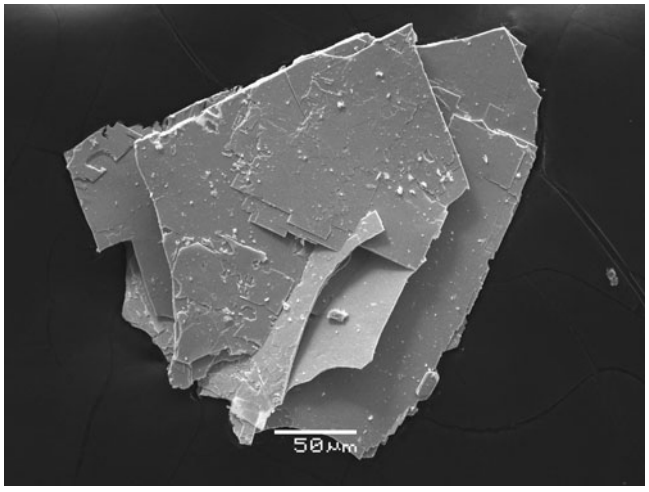

Figure 1. Cluster of lamellar napoliite crystals. Scanning electron microscopy (back-scattered electron) image. Sample # 5885/1.

Table 1. Reflectance data (R, %) of napoliite.*

R_{max} (%)	R_{min} (%)	λ (nm)	R_{max} (%)	R_{min} (%)	λ (nm)
15.8	14.8	400	15.1	14.0	560
15.7	14.7	420	14.9	13.9	580
15.4	14.4	440	**14.9**	**13.8**	**589**
15.3	14.3	460	14.8	13.6	600
15.3	**14.3**	**470**	14.7	13.4	620
15.3	14.3	480	14.7	13.3	640
15.3	14.3	500	**14.7**	**13.3**	**650**
15.3	14.3	520	14.6	13.2	660
15.2	14.1	540	14.6	13.2	680
15.2	**14.1**	**546**	14.4	13.1	700

*The values required by the Commission on Ore Mineralogy are given in bold.

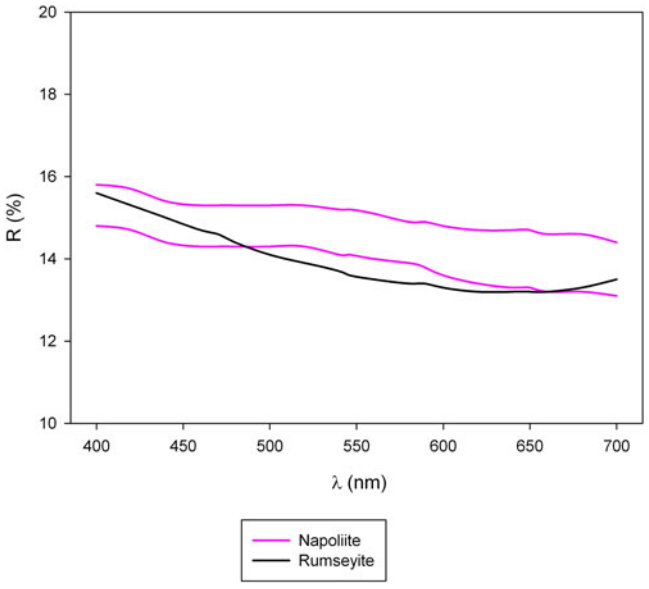

Figure 2. Reflectivity curves for napoliite compared with the published data for rumseyite (Turner *et al.*, 2012).

https://doi.org/10.1180/mgm.2023.43 Published online by Cambridge University Press

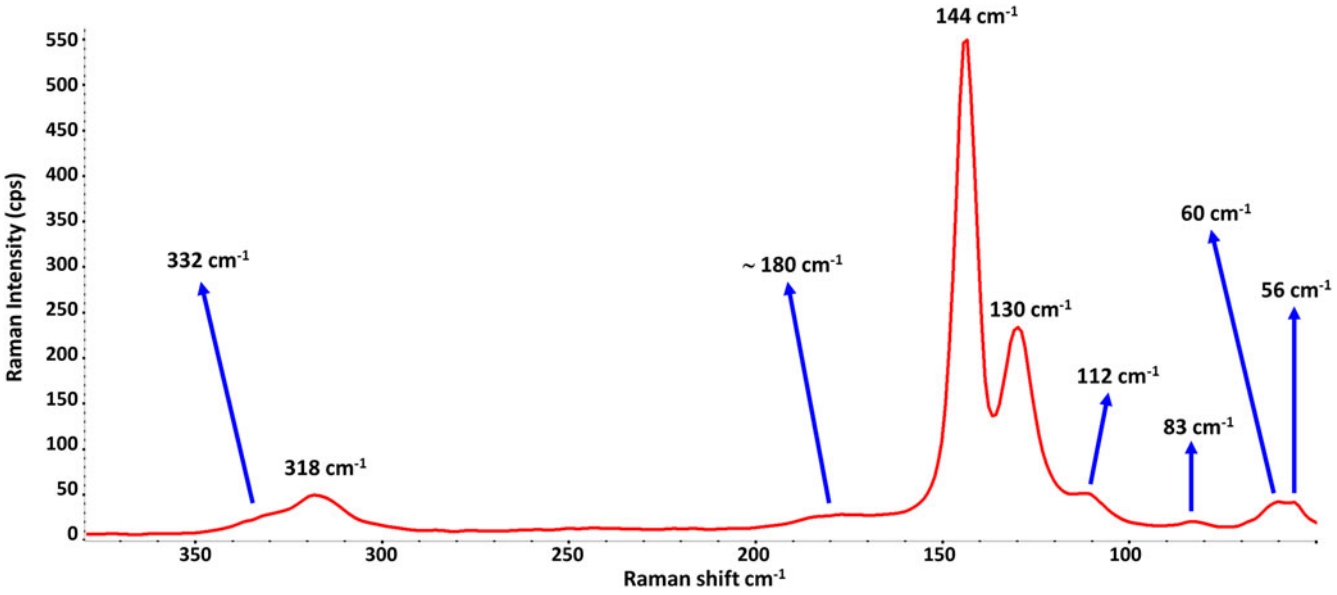

Figure 3. Raman spectrum of napoliite excited by 532 nm laser.

Napoliite is optically uniaxial. Its refractive indices (RI) could not be measured because of the absence of immersion liquids that can measure RI values higher than 2.0. The Gladstone–Dale relationship predicts an average RI of 2.10 which is similar to that of other Pb oxychloride minerals [e.g. 2.13 for blixite $Pb_8O_5(OH)_2Cl_4$ (Gabrielson *et al.*, 1958; Krivovichev and Burns, 2006); 2.27 for yeomanite $Pb_2O(OH)Cl$ (Turner *et al.*, 2015); 2.32 for damaraite $Pb_3O_2(OH)Cl$ (Criddle *et al.*, 1990)]. Optical properties of napoliite were studied using the methods common for metallic minerals. In reflected light, napoliite is grey with no visible bireflectance and pleochroism. In crossed polars it is very weakly anisotropic. Internal reflections are not observed. The set of reflectance measurements performed in air relative to a SiC standard by means of a Universal Microspectrophotometer UMSP 50 (Opton-Zeiss, Germany) is given in Table 1 and plotted in Fig. 2 in comparison with the published data for rumseyite (Turner *et al.*, 2012).

Raman spectroscopy

The Raman spectrum of napoliite (Fig. 3) was collected in the range 50–400 cm^{-1} as no peaks were observed above 350 cm^{-1}. The data were collected using a DXR Thermo Scientific Raman spectrometer, equipped with a diode-pumped solid-state 532 nm laser. The analytical points were performed with a 50× LWD (long working distance) objective, operating at a power of 4 mW, with a spectral resolution in the range of ~3 cm^{-1} and a spatial resolution of ~1 μm. The acquisition time adopted was 10 s for 10 scans accumulation.

Table 2. Chemical composition of napoliite (wt.%, mean of seven analyses).

Constituent	Wt.%	Range	S.D.	Standard
PbO	91.71	91.49–91.85	0.12	PbTe
F	3.89	3.71–4.07	0.12	MgF_2
Cl	7.34	7.27–7.40	0.04	NaCl
–O = F+Cl	–3.30			
Total	99.64			

S.D. – standard deviation

The Raman spectrum of napoliite shows two very intense peaks at 144 and 130 cm^{-1}, whereas lower intensity peaks are positioned in the region between about 315 and 330 cm^{-1}, and

Table 3. Powder X-ray diffraction data (*d* in Å) of napoliite. The eight strongest lines are given in bold.

I_{obs}	d_{obs}	I_{calc}*	d_{calc}**	*h k l*
12	6.28	11	6.262	002
6	5.74	4	5.742	100
85	**3.860**	51	3.862	111
20	**3.139**	13	3.131	004
100	**2.914**	100	2.911	113
63	**2.866**	45	2.871	200
2	2.610	0.5	2.610	202
2	2.563	1	2.568	210
3	2.514	2	2.515	211
4	2.191	4	2.187	213
19	**2.118**	27	2.116	204
9	2.094	5	2.087	006
19	**2.027**	21	2.030	220
2	1.929	2	1.931	222
2	1.915	2	1.914	300
10	1.795	10	1.797	311
4	1.704	8	1.703	224
9	1.692	13	1.688	206
20	**1.665**	30	1.665	313
23	**1.642**	13	1.637	117
1	1.593	2	1.592	320
5	1.571	1	1.566	008
1	1.487	1	1.488	323
2	1.472	0.5, 1	1.470, 1.468	315, 217
4	1.458	5	1.455	226
4	1.435	5	1.435	400
1	1.421	1	1.419	324
1	1.399	0.5	1.399	402
4	1.378	1, 2	1.384, 1.374	411, 208
2	1.345	2	1.346	331
6	1.321	3, 2	1.321, 1.316	413, 119
2	1.305	3	1.305	404
4	1.284	6, 5	1.287, 1.284	333, 420
8	1.277	10	1.274	317

*For the calculated pattern, only reflections with intensities ≥0.5 are given.
**For the unit-cell parameters obtained by single-crystal X-ray diffraction.

https://doi.org/10.1180/mgm.2023.43 Published online by Cambridge University Press

Table 4. Crystallographic data and refinement parameters for napoliite.

Crystal data	
Space group	$P4_2/mcm$
Unit cell dimensions a, c (Å)	5.7418(11), 12.524(4)
Unit cell volume (Å^3)	412.9(2)
Absorption coefficient (mm^{-1})	81.909
Crystal size (mm)	0.05 × 0.05 × 0.005
Data collection	
Temperature (K)	293
Radiation, wavelength (Å)	Mo$K\alpha$, 0.71073
θ range (°)	3.548–27.971
h, k, l ranges	−7→6, −7→7, −15→16
Total reflections collected	2961
Unique reflections (R_{int})	300 (0.05)
Unique reflections $F > 4\sigma(F)$	222
Structure refinement	
Refinement method	Full-matrix least-squares on F^2
Weighting coefficients a, b	0.0417, 0.196
Data/restraints/parameters	300/0/20
R_1 [$F > 4\sigma(F)$], wR_2 [$F > 4\sigma(F)$]	0.024, 0.063
R_1 all, wR_2 all	0.035, 0.070
Gof on F^2	1.090
Largest diff. peak and hole (e^- Å^{-3})	2.479, −1.816

even lower intensity peaks at about 180, 112, 83, 60 and 56 cm^{-1}. No Raman signals are detected for those regions above 350 cm^{-1} including the OH$^-$ region above 3000 cm^{-1}.

The Raman spectra of synthetic compounds related structurally to napoliite are unknown. In addition, the Raman spectrum of its polymorph rumseyite is also unreported. However, we can compare the napoliite Raman spectrum with the F-free synthetic compound $Pb_3O_2Cl_2$ described by Zakir′yanov *et al.* (2016). On the basis of this work, the peaks in the 130–150 cm^{-1} region of napoliite could be assigned to the Pb–Cl stretching vibrations and the peaks in the 315–330 cm^{-1} region to the Pb–O stretching vibrations. However, the strongest peak in the Raman spectrum of litharge, along with another strong peak at 339 cm^{-1}, is observed at 146 cm^{-1} (Ciomartan *et al.*, 1996). Thus, the peak at 144 cm^{-1} may be a superposition of the bands of Pb–Cl-stretching and O–Pb–O-bending vibrations.

However, an alternative interpretation of the Raman spectrum of napoliite in the range 110–150 cm^{-1} is possible. The vibrational mode, which corresponds to the most intense band with the wavenumber $k_w = 144$ cm^{-1}, belongs to the ground vibrational state (zeroth vibrational level). At room temperature, the corresponding normal vibrations are partially excited. The fractions of Pb–O bonds located at the first and second vibrational levels (without taking into account anharmonicity) are $p_1 = \exp[-(h\nu)/(kT)]$ and $p_2 = \exp[-(2h\nu)/(kT)]$ of the fraction of the unexcited state, respectively, where h is the Planck constant, $\nu = ck_w$ is the frequency (c is the speed of light in vacuum), k is the Boltzmann constant and T is temperature. According to the relationship $h\nu = kT_{eq}$, the temperature T_{eq} of 298 K is equivalent to the wavenumber kw^{298} of 207 cm^{-1}, and the values of p_1 and p_2 are equal to 0.5 and 0.25, respectively. Considering that the polarisability (and hence the intensity of Raman scattering) depends on the anharmonicity, it can be assumed that the bands at 139 and 112 cm^{-1} refer to thermally excited states at the first and second vibrational levels with anharmonic shifts of 14 and 32 cm^{-1}, respectively.

Table 6. Selected interatomic distances (Å) in napoliite.

Pb1–O1	2.2915(6)
Pb1–O/F1	2.4129(5) ×2
Pb1–F1	2.5286(7)
Pb1–Cl1	3.251(2) ×2
Pb1–Cl1	3.566(2) ×2

On the basis of data from Zakir′yanov *et al.* (2016), the peaks at 112 and 180 cm^{-1} are assigned to the O–Pb–O bending vibrations and the peaks at 56, 60 and 83 cm^{-1} to Cl–Pb–O, Cl–Pb–F and Cl–Pb–F bending vibrations. Comparison with Raman spectra of oxygen-free lead halides are generally in agreement with the assignment made by Zakir′yanov *et al.* (2016). No known Raman spectra of lead chlorides and fluorides contain bands of fundamental modes above 240 cm^{-1}, whereas such bands are observed in Raman spectra of the Pb^{2+} oxides, litharge (at 321 and 339 cm^{-1}: Ciomartan *et al.*, 1996; Madsen and Weaver, 1998 and massicot (at 289 and 384 cm^{-1}: Ciomartan *et al.*, 1996; Madsen and Weaver, 1998) and also mendipite, $Pb_3O_2Cl_2$ (at 330 cm^{-1}: Bouchard and Smith, 2003). Thus, the bands at 318 and 332 cm^{-1} in the Raman spectrum of napoliite should be assigned to stretching vibrations of the longer and the shorter Pb–O bonds, respectively (see Table 6).

Bands with the largest Raman shift of 202 cm^{-1} are observed in the Raman spectra of lead chlorides cotunnite, $PbCl_2$, and challacolloite, KPb_2Cl_5. However, these bands correspond to overtones (e.g. the strongest fundamental stretching band of cotunnite is observed at ∼100 cm^{-1}: Bouchard and Smith, 2003). Raman spectra of fluorocronite, PbF_2 (Krishnamurthy and Soots, 1970) and matlockite, PbFCl (Bouchard and Smith, 2003) contain distinct bands in the range 220–260 cm^{-1}. These bands are absent in the Raman spectrum of napoliite. Consequently, bands below 200 cm^{-1} in Fig. 3 can be assigned tentatively to mixed soft lattice modes involving both Pb–F and Pb–Cl bonds as well as Cl–Pb–O and F–Pb–O angles.

Bands in the range 590–700 cm^{-1} and at 447 cm^{-1} in the infrared spectrum of fiedlerite–1A, $Pb_3Cl_4F(OH)\cdot H_2O$ are assigned to the Pb···O–H bending and H_2O libration vibrations (Zubkova *et al.*, 2019). Thus, the absence of bands above 340 cm^{-1} in the Raman spectrum of napoliite is in agreement with the conclusion on the absence of OH groups and H_2O molecules in this mineral.

Table 5. Coordinates and displacement parameters (Å) of atoms in napoliite.

Site	Wyk.	x	y	z	U_{eq}	U^{11}	U^{22}	U^{33}	U^{23}	U^{13}	U^{12}
Pb1	8*o*	0.73266(7)	0.73266(7)	0.35353(4)	0.0180(3)	0.0190(3)	0.0190(3)	0.0160(4)	−0.00054(10)	−0.00054(10)	−0.0094(2)
Cl1	4*i*	0.7348(5)	0.2652(5)	½	0.0287(12)	0.0244(15)	0.0244(15)	0.037(4)	0	0	0.013(2)
F1	2*b*	0	0	¼	0.019(7)	0.010(5)	0.010(5)	0.04(2)	0	0	0
O/F1*	4*e*	0	½	¼	0.018(6)	0.022(7)	0.026(7)	0.005(18)	0	0	0
O1	2*d*	½	½	¼	0.014(8)	0.008(6)	0.008(6)	0.03(2)	0	0	0

*$O_{0.5}F_{0.5}$

https://doi.org/10.1180/mgm.2023.43 Published online by Cambridge University Press

Chemical composition and chemical properties

Seven electron-microprobe analyses were carried out with a JEOL JXA 8230 Superprobe (wavelength dispersive spectroscopy mode with an accelerating voltage of 20 kV, a beam current on the specimen of 20 nA and a beam diameter of 2 μm). Peak counting times (CT) were 20 s for all elements; CT for each background was one-half of the peak time. The raw intensities were converted into concentrations using *X-PHI* (Merlet, 1994) matrix-correction software. Both the crystal structure data and Raman spectroscopy confirm the absence of H_2O and OH, borate and carbonate groups in the mineral. The contents of

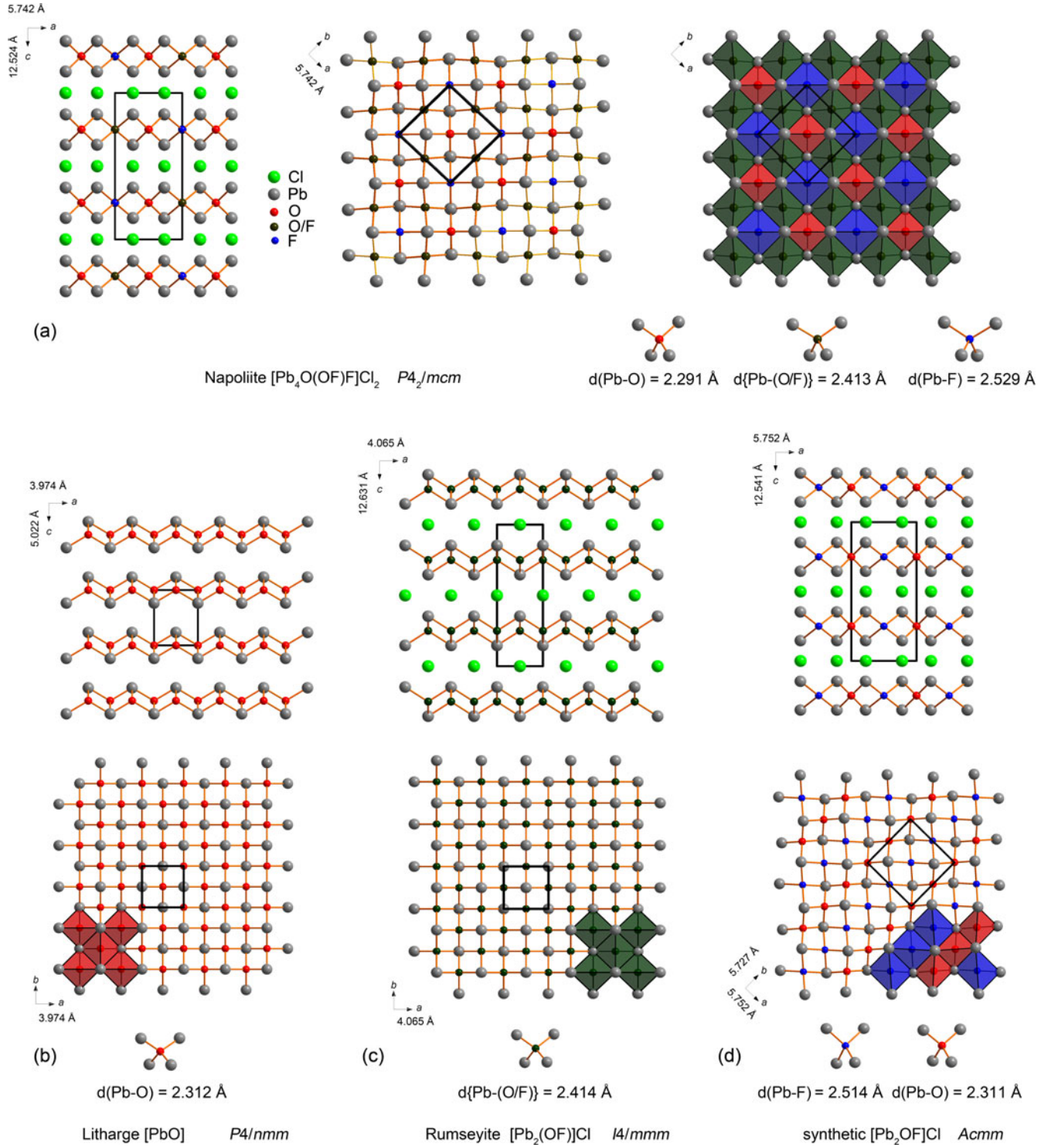

Figure 4. The crystal structures in balls-and-sticks and polyhedral representations of (a) napoliite; (b) structurally related litharge (Boher *et al.*, 1985); (c) rumseyite (Turner *et al.*, 2012); and (d) synthetic [Pb2OF]Cl (Aurivillius, 1977). In structural formulae, litharge-derived blocks are given in square brackets. Average Pb–*X* (*X* = O, F) bond lengths in XPb_4 anion-centred tetrahedra are given for each crystal structure. Designations: grey balls = Pb; green balls = Cl; red balls = O sites; blue balls = F sites; dark green = mixed O/F sites; OPb_4 tetrahedra = red; $(O/F)Pb_4$ tetrahedra = dark green and FPb_4 = blue. Pb–Cl long bonds are omitted for clarity.

https://doi.org/10.1180/mgm.2023.43 Published online by Cambridge University Press

other elements with atomic numbers higher than that of carbon are below detection limits. Analytical data and standards used are given in Table 2.

The empirical formula calculated on the basis of 3 anions is $Pb_{1.999}O_{0.997}F_{0.996}Cl_{1.007}$. The ideal formula is Pb_2OFCl, which requires PbO 92.07, F 3.92, Cl 7.31, –O ≡ F+Cl –3.30, total 100 wt.%.

Napoliite is slowly soluble in dilute hydrochloric acid without gas evolution.

X-ray diffraction data and crystal structure

The powder X-ray diffraction (XRD) data (Table 3) were collected with a Rigaku R-AXIS Rapid II diffractometer equipped with cylindrical image plate detector using the Debye-Scherrer geometry (d = 127.4 mm), Co$K\alpha$ radiation (rotating anode with VariMAX microfocus optics), 40 kV, 15 mA, and an exposure time of 15 min. The angular resolution of the detector is 0.045 2θ (pixel size 0.1 mm). The data were integrated using the software package *Osc2Tab* (Britvin *et al.*, 2017). The unit-cell parameters refined from the powder data using *UNITCELL* software by Holland and Redfern (1997) are as follows: napoliite is tetragonal, space group $P4_2/mcm$, a = 5.737(1), c = 12.573(3) Å, V = 413.8(2) Å^3 and Z = 4.

To obtain the single-crystal XRD data a thin lamellar crystal of napoliite was mounted on a thin glass fibre and examined using Bruker APEX II DUO X-ray diffractometer with a Mo-IμS microfocus X-ray tube (λ = 0.71073 Å) operated at 50 kV and 0.6 mA. More than a hemisphere of three-dimensional XRD data was collected with frame widths of 0.5° in ω, and a 120 s count time for each frame. Then the collected data were integrated and corrected for absorption using a multi scan type model implemented in the Bruker programs *APEX* and *SADABS* (Bruker-AXS, 2014). The unit-cell parameters of napoliite [a = 5.7418(11), c = 12.524(4) Å, V = 412.9(2) Å^3 and Z = 4 in $P4_2/mcm$] were determined and refined by least-squares techniques. The crystal structure was refined using *SHELXL* (Sheldrick, 2015) to R_1 = 0.024 for 222 reflections with $F > 4\sigma(F)$. Crystallographic data and refinement parameters are reported in Table 4; coordinates and displacement parameters of atoms in Table 5 and selected interatomic distances in Table 6. The crystallographic information file has been deposited with the Principal Editor of *Mineralogical Magazine* and is available as Supplementary material (see below).

All attempts to refine the structure of napoliite in orthorhombic space groups, as reported earlier for synthetic $[Pb_2OF]Cl$ (Aurivillius, 1977), resulted in physically unrealistic displacement parameters for Pb, Cl and O atoms and instability of the refinement.

The structure of napoliite (Fig. 4a) contains one symmetrically unique Pb position. The Pb^{2+} cation is coordinated by one O, one F, two mixed O/F sites and four Cl atoms (Table 6). The coordination geometry of the Pb atom in napoliite can be described as a distorted square antiprism. In agreement with previous results on Pb oxychlorides, the general feature of the Pb^{2+} coordination in napoliite is the presence of several short Pb–X (X = O and F) bonds [2.2915(6)–2.5286(7) Å] located in one coordination hemisphere of the Pb^{2+} cation. In the opposite hemisphere, the Pb^{2+} cation forms four long Pb–Cl bonds [3.251(2)–3.566(2) Å]. This distortion is interpreted as the influence of the stereoactivity of the s^2 lone electron pair on the Pb^{2+} cation.

The Cl atoms have cubic coordination, whereas all X sites have tetrahedral coordination (Siidra *et al.*, 2008), thus being central for anion-centred OPb_4, FPb_4 and $(O/F)Pb_4$ tetrahedra (Fig. 4a). XPb_4 tetrahedra in napoliite are characterised by typical bond-length values (Table 6 and Fig. 4a). In napoliite, O1 atom forms four O–Pb bonds of 2.2915(6) Å each, which is in a good agreement with the average bond length value of 2.33 Å in ideal OPb_4 tetrahedra observed for well refined structures (Krivovichev *et al.*, 2013). The mixed oxygen/fluorine O/F1 site is tetrahedrally coordinated by four Pb–(O/F) bonds of 2.4129(5) Å, which is almost identical with the average Pb–(O/F) bond length of 2.41 Å in rumseyite (Turner *et al.*, 2012). The presence of a site occupied by F in the crystal structure of napoliite is confirmed by the Pb–F bond length of 2.5286(7) Å. Anion-centred FPb_4 tetrahedra are also present in the structure of grandreefite, $Pb_2(SO_4)F_2$ (Kampf, 1991). The average F–Pb bond length in its structure is 2.55 Å.

Table 7. Comparative data for napoliite and rumseyite.

Mineral	Napoliite	Rumseyite
Ideal formula	Pb_2OFCl	Pb_2OFCl
Structural formula	$[Pb_4O(OF)F]Cl_2$	$[Pb_2(OF)]Cl$
Crystal system	Tetragonal	Tetragonal
Space group	$P4_2/mcm$	$I4/mmm$
a (Å)	5.7418(11)	4.065(1)
c (Å)	12.524(4)	12.631(7)
V (Å^3)	412.9(2)	208.7(1)
Z	4	2
Strongest lines of the powder X-ray diffraction pattern:		
d (Å) – I (%)	3.860–85	6.306–17
	3.139–20	3.848–41
	2.914–100	2.923–100
	2.866–63	2.875–68
	2.118–19	2.110–12
	2.027–19	2.049–10
	1.665–20	1.719–9
	1.642–23	1.680–14
Colour	Colourless	Pale orange-brown
Streak	White	White
Transparency	Transparent	Translucent
Tenacity	Brittle	Brittle
Cleavage	Perfect on {001}	Perfect on {100}
Density (calc.) (g cm^{-3})	7.797	7.838*
Mean refractive index (calculated at 589 nm)	2.10	2.106*
COM reflectance values (%)**		
470 nm	14.3/15.3	14.6
546 nm	14.1/15.2	13.6
589 nm	13.8/14.9	13.4
650 nm	13.3/14.7	13.2
Source	This paper	Turner *et al.* (2012)

*Calculated by us from the chemical composition and unit cell parameters of rumseyite given by Turner *et al.* (2012)
**R_{min}/R_{max} for napoliite, R for rumseyite

Discussion

Napoliite is a new representative (Fig. 4a) of a family of layered lead oxychlorides with lead oxide blocks derived from litharge PbO (Fig. 4b) (Boher *et al.*, 1985; Chukanov *et al.*, 2019). The structure of napoliite shows that the litharge-derived blocks may have different degrees and arrangements of F substitutions for O.

Napoliite is dimorphous with rumseyite (Turner *et al.*, 2012). Both minerals have not only identical chemical composition but also many similar physical properties. It should be noted that some properties of rumseyite (density, mean refractive index) were calculated erroneously by Turner *et al.* (2012); we use this occasion to correct these data (Table 7).

https://doi.org/10.1180/mgm.2023.43 Published online by Cambridge University Press

However, the crystal structures of these minerals, their space groups and powder X-ray diffraction patterns are different (Table 7, Fig. 4). Their origin is also different. Rumseyite is a secondary mineral formed due to the decomposition of galena in manganese oxide pods distributed in Carboniferous Limestone at the Torr Works (Merehead) Quarry in England, whereas napoliite is a fumarolic mineral deposited directly from hot gas as a volcanic sublimate. Both minerals can be considered as extremely rare; they have been found in a single specimen each and neither has a known, reliably characterised synthetic analogue.

From the crystal chemical point of view, a specific feature of rumseyite, $[Pb_2(OF)]Cl$, is that all O^{2-} anions in the [PbO] block are partially substituted by F^- (Fig. 4c). In synthetic orthorhombic Pb_2OFCl (Aurivillius, 1977), F and O atoms are completely ordered over two symmetrically independent anionic sites (Fig. 4d). Thus, napoliite represents a new structure type with a unique order/disorder pattern of fluorine and oxygen atoms. Its structural formula is $[^{Pb1}Pb_4{}^{O1}O^{O/F1}(OF)^{F1}F]^{Cl1}Cl_2$, where the litharge-derived block is in square brackets.

Acknowledgements. We acknowledge Mike Rumsey and three anonymous reviewers, Associate Editor Elena Zhitova and Principal Editor Stuart Mills for valuable comments. Technical support by the SPbSU X-ray Diffraction Resource Centre is gratefully acknowledged. Interpretation of the Raman spectrum was performed in accordance with the state task, state registration No. AAAA-A19-119092390076-7.

Supplementary material. The supplementary material for this article can be found at https://doi.org/10.1180/mgm.2023.43.

Competing interests. The authors declare none.

References

Alfano G.B. and Parascandola A. (2015) *Il Vesuvio e le sue eruzioni. Dagli appunti lasciati dagli autori. A cura di Corrado Buondonno, Con il commento di Giuseppe Luongo*. Doppiavoce, Napoli, Italy, 462 pp. [in Italian].

Aurivillius B. (1977) A case of mimetic twinning the crystal structure of Pb_2OFX (X = Cl, Br and I). *Chemica Scripta*, **11**, 208–210.

Balić-Žunić T., Garavelli A., Pinto D. and Mitolo D. (2018) Verneite, $Na_2Ca_3Al_2F_{14}$, a new aluminum fluoride mineral from Icelandic and Vesuvius fumaroles. *Minerals*, **8**, 553.

Boher P., Garnier P., Gavarri J.R. and Hewat A.W. (1985) Monoxyde quadratique PbOα(I): Description de la transition structurale ferroélastique. *Journal of Solid State Chemistry*, **57**, 343–350.

Bouchard M. and Smith D.C. (2003) Catalogue of 45 reference Raman spectra of minerals concerning research in art history or archaeology, especially on corroded metals and coloured glass. *Spectrochimica Acta A*, **59**, 2247–2266.

Britvin S.N., Dolivo-Dobrovolsky D.V. and Krzhizhanovskaya M.G. (2017) Software for processing the X-ray powder diffraction data obtained from the curved image plate detector of Rigaku RAXIS Rapid II diffractometer. *Zapiski Rossiiskogo Mineralogicheskogo Obshchestva*, 146, 104–107 [in Russian].

Campostrini I. and Gramaccioli C. (2005) Artroeite del Monte Somma-Vesuvio: secondo ritrovamento mondiale. *Rivista Mineralogica Italiana*, **29**, 50–52 [in Italian].

Campostrini I., Demartin F. and Russo M. (2019) Sbacchiite, Ca_2AlF_7, a new fumarolic mineral from the Vesuvius volcano, Napoli, Italy. *European Journal of Mineralogy*, **31**, 153–158.

Campostrini I., Castellano C., Demartin F., Rocchetti I., Russo M. and Vignola P. (2022) Paradimorphite, β-As_4S_3, a vintage new mineral from Solfatara di Pozzuoli and Vesuvius, Napoli, Italy. *Mineralogical Magazine*, **86**, 500–506.

Chukanov N.V., Siidra O.I., Polekhovsky Yu.S., Pekov I.V., Varlamov D.A., Ermolaeva V.N. and Virus A.A. (2019) Erikjonssonite, $(Pb_{32}O_{21})[(V,Si,Mo,As)O_4]_4Cl_9$, a new mineral from the Kombat mine and structural classification of layered lead oxychlorides related to litharge. *European Journal of Mineralogy*, **31**, 619–628.

Ciomartan D.A., Clark R.J.H., McDonald L.J. and Oldyha M. (1996) Studies on the thermal decomposition of basic lead(II) carbonate by Fourier-transform Raman spectroscopy, X-ray diffraction and thermal analysis. *Journal of Chemical Society, Dalton Transactions*, **18**, 3639–3645.

Criddle A.J., Keller P., Stanley C.J. and Innes J. (1990) Damaraite, a new lead oxychloride mineral from the Kombat mine, Namibia (South West Africa). *Mineralogical Magazine*, **54**, 593–598.

Demartin F., Campostrini I., Castellano C., Gramaccioli C.M. and Russo M. (2012) D'ansite-(Mn), $Na_{21}Mn^{2+}(SO_4)_{10}Cl_3$ and d'ansite-(Fe), $Na_{21}Fe^{2+}(SO_4)_{10}Cl_3$, two new minerals from volcanic fumaroles. *Mineralogical Magazine*, **76**, 2773–2783.

Demartin F., Campostrini I., Castellano C. and Russo M. (2014) Parascandolaite, $KMgF_3$, a new perovskite-type fluoride from Vesuvius. *Physics and Chemistry of Minerals*, **41**, 403–407.

Gabrielson O., Parwel A. and Wickman F.E. (1958) Blixite, a new lead-oxyhalide mineral from Långban. *Arkiv för Mineralogi och Geologi*, **2**, 411–415.

Holland T.J.B. and Redfern S.A.T. (1997) Unit cell refinement from powder diffraction data: the use of regression diagnostics. *Mineralogical Magazine*, **61**, 65–77.

Kampf A.R. (1991) Grandreefite, $Pb_2F_2SO_4$: crystal structure and relationship to the lanthanide oxide sulfates, $Ln_2O_2SO_4$. *American Mineralogist*, **76**, 278–282.

Kasatkin A.V., Siidra O.I., Nestola F., Pekov I.V., Agakhanov A.A., Nazarchuk E.V., Koshlyakova N.N., Chukanov N.V. and Rossi M. (2023) Napoliite, IMA 2022-073. CNMNC Newsletter 70, *Mineralogical Magazine*, **87**, 160–168.

Krishnamurthy N. and Soots V. (1970) Raman spectra of CdF_2 and PbF_2. *Canadian Journal of Physics*, **48**, 1104–1107.

Krivovichev S.V. and Burns P.C. (2006) The crystal structure of $Pb_8O_5(OH)_2Cl_4$, a synthetic analogue of blixite? *The Canadian Mineralogist*, **44**, 515–522.

Krivovichev S.V., Mentré O., Siidra O.I., Colmont M. and Filatov S.K. (2013) Anion-centered tetrahedra in inorganic compounds. *Chemical Reviews*, **113**, 6459–6535.

Lima A., De Vivo B., Fedele L., Sintoni F. and Milia A. (2007) Geochemical variations between the 79 A.D. and 1944 A.D. Somma-Vesuvius volcanic products: constraints on the evolution of hydrothermal system based on fluid and melt inclusions. *Chemical Geology*, **237**, 401–417.

Madsen L.D. and Weaver L. (1998) Characterization of lead oxide thin films produced by chemical vapor deposition. *Journal of American Ceramical Society*, **81**, 988–996.

Malcherek T., Bindi L., Dini M., Ghiara M.R., Molina Donoso A., Nestola F., Rossi M. and Schlüter J. (2014) Tondiite, $Cu_3Mg(OH)_6Cl_2$, the Mg-analogue of herbertsmithite. *Mineralogical Magazine*, **78**, 583–590.

Melluso L., Scarpati C., Zanetti A., Sparice D. and de' Gennaro R. (2022) The petrogenesis of chemically zoned, phonolitic, Plinian and sub-Plinian eruptions of Somma-Vesuvius, Italy: Role of accessory phase removal, independently filled magma reservoirs with time, and transition from slightly to highly silica undersaturated magmatic series in an ultrapotassic stratovolcano. *Lithos*, **430–431**, 106854.

Merlet C. (1994) An accurate computer correction program for quantitative electron probe microanalysis. *Microchimica Acta*, **114/115**, 363–376.

Nestola F., Kasatkin A.V., Biagioni C., Škoda R., Santello L. and Agakhanov A.A. (2023) Manuelarossiite, IMA 2022–097, in: CNMNC Newsletter 71. *European Journal of Mineralogy*, **35**, 75–79.

Parascandola A. (1951) I minerali del Vesuvio nella eruzione del marzo 1944 e quelli formati durante l'attuale periodo diriposo. *Bollettino della Società Geologica Italiana*, **70**, 523–526 [in Italian].

Parascandola A. (1960) Notizie vesuviane. Il Vesuvio dal marzo 1948 al dicembre 1958. *Bollettino della Società dei Naturalisti in Napoli*, **68**, 1–184 [in Italian].

Parascandola A. (1961) Notizie vesuviane. Il Vesuvio dal gennaio 1959 al dicembre 1960. *Bollettino della Società dei Naturalisti in Napoli*, **69**, 263–298 [in Italian].

Rossi M., Nestola F., Zorzi F., Lanza A., Peruzzo L., Guastoni A. and Kasatkin A. (2014) Ghiaraite: A new mineral from Vesuvius volcano, Naples (Italy). *American Mineralogist*, **99**, 519–524.

Russo M. and Campostrini I. (2011) Ammineite, matlockite and post 1944 eruption fumarolic minerals at Vesuvius. *Plinius*, **37**, 312.

Russo M., Campostrini I. and Demartin F. (2014) Fumarolic minerals after the 1944 Vesuvius eruption. Abstract in: *The Future of the Italian Geosciences – The Italian Geosciences of the Future* (Cesare B., Erba E., Carmina B., Fascio L., Petti F.M. and Zuccari A., editors). Abstract Book, 87° Congresso della Società Geologica Italiana e 90° Congresso della Società Italiana di Mineralogia e Petrologia, Milan, Italy, September 10–12, 2014. *Rendiconti Online della Società Geologica Italiana*, **31**, Supplemento n. 1.

Santacroce R., Cioni R., Marianelli P., Sbrana A., Sulpizio R., Zanchetta G., Donahue D.J. and Joron J.L. (2008) Age and whole rock-glass composition of proximal pyroclastics from the major explosive eruptions of Somma-Vesuvius: a review as a tool for distal tephrostratigraphy. *Journal of Volcanology and Geothermal Research*, **177**, 1–18.

Sbrana A., Cioni R., Marianelli P., Sulpizio R., Andronico D. and Pasquini G. (2020) Volcanic evolution of the Somma-Vesuvius Complex (Italy). *Journal of Maps*, **16**, 137–141.

Sheldrick G.M. (2015) Crystal structure refinement with SHELXL. *Acta Crystallographica*, **A71**, 3–8.

Siidra O.I., Krivovichev S.V. and Filatov S.K. (2008) Minerals and synthetic Pb (II) compounds with oxocentered tetrahedra: review and classification. *Zeitschrift für Kristallographie – Crystalline Materials*, **223**, 114–126.

Turner R.W., Siidra O.I., Krivovichev S.V., Stanley C.J. and Spratt J. (2012) Rumseyite, $[Pb_2OF]Cl$, the first naturally occurring fluoroxychloride mineral with the parent crystal structure for layered lead oxychlorides. *Mineralogical Magazine*, **76**, 1247–1255.

Turner R.W., Siidra O.I., Rumsey M.S., Polekhovsky Y.S., Kretser Y.L., Krivovichev S.V., Spratt J. and Stanley C.J. (2015) Yeomanite, $Pb_2O(OH)Cl$, a new chain-structured Pb oxychloride from Merehead Quarry, Somerset, England. *Mineralogical Magazine*, **79**, 1203–1211.

Zakir′yanov D.O., Chernyshev V.A. and Zakir′yanova I.D. (2016) Phonon spectrum of lead oxychloride $Pb_3O_2Cl_2$: Ab initio calculation and experiment. *Physics of the Solid State*, **58**, 325–332.

Zubkova N.V., Chukanov N.V., Pekov I.V., Pushcharovsky D.Yu., Katerinopoulos A., Voudouris P. and Magganas A. (2019) New data on fiedlerite–1*A* from ancient slags of Lavrion, Greece: crystal structure and hydrogen bonding. *Doklady Earth Sciences*, **486**, 517–520.

https://doi.org/10.1180/mgm.2023.43 Published online by Cambridge University Press